Symmetry-mode Refinements

Prof. John S.O. Evans, Department of Chemistry, Durham University, Lower Mount Joy, South Rd,, Durham, DH1 3LE, UK.

1. Introduction/overview

These notes introduce the topic of symmetry- or distortion-mode refinements,[1-2] which offer a convenient, concise and systematic way of studying compounds that undergo structural phase transitions. We will use the language of the ISODISTORT suite of tools developed and maintained by Branton Campbell and Harold Stokes (https://stokes.byu.edu/iso/isodistort.php),[3] which interfaces with major Rietveld software packages such as TOPAS, Fullprof and GSAS. Similar and complementary tools are available via the Bilbao crystallagraphic server (https://www.cryst.ehu.es/cryst/amplimodes.html).

2. Symmetry-changing phase transitions

Many technologically important materials show changes in their properties (conductivity, magnetism, ferroelectricity, piezoelectricity, optical properties, etc) associated with phase transitions. We can loosely divide phase transitions into two categories: *reconstructive* and *non-reconstructive*. In the former, significant changes in bonding mean that the structures before and after the transition are very different, and are best considered separately. In the latter, the changes in structure are often small (minor displacements in atomic coordinates or rotations of groups of atoms), despite have a significant impact on properties, and it can be useful to describe one structure relative to the other. The structural changes lead to a change in space-group symmetry between what are called the *parent* (more formally *aristotype*) and the *child* (*hettotype*) structures. Usually the higher-symmetry parent is a high temperature (or low pressure) form which transitions to a lower-symmetry child form on cooling, but this is not a thermodynamic requirement.[4-5]

Several other lectures have discussed how it is often necessary to bring extra information to structural analysis from powder diffraction data. The symmetry-mode approach gives us another opportunity for this by exploiting the relationship between parent and child structures. In a conventional crystallographic approach the lower-symmetry child is described by refining *xyz* coordinates without reference to the parent. In the symmetry-mode approach, we describe the child structure in terms of the high-symmetry parent structure plus the amplitude of so-called symmetry adapted distortion modes. The amplitude of a mode (a single Rietveld parameter) typically affects multiple atoms in the child structure, which can lead to very concise (low parameter number) structural descriptions.[1-2, 6]

We will explore these ideas using WO_3 – the fruit-fly of phase transitions – in Section 3, but it's useful to have a simple picture in mind before doing that. If you've got a chemistry background, think about how you might describe a distorted water molecule with one short and one long O–H bond rather than its usual symmetric structure (point group C_{2v}). One way would be to quote *xyz* coordinates for each H relative to the O. A more efficient way might be to remember that the normal modes of vibration of H_2O can be described by an a_1 symmetric bond stretch, a b_1 asymmetric bond stretch, and an a_1 bending mode. The distorted molecule could then be described in terms of the undistorted form plus the amplitude of a frozen-in b_1 asymmetric stretch. Note that freezing in the a_1 symmetric stretch or a_1 bend wouldn't lower the symmetry from C_{2v}, but the b_1 does. a_1 is called the totally symmetric irreducible representation. Freezing in a mode with a different irreducible representation is a recipe for symmetry lowering (here to C_s).

One advantage of the symmetry-mode approach is that the parameters refined are often directly related to the specific structural distortions occurring at the phase transition. In metal oxide chemistry, for example, they often describe processes such as Jahn–Teller distortions of octahedra, or coupled rotations of linked MO_6 octahedra. This arises because the free energy change associated with a phase transition can be expressed in Landau theory in terms of the order parameters of the irreducible representations of the parent space group symmetry (these

terms are defined in Section 3.2).[7] Often only a small number of these order parameters (frequently only one) dominate the free energy change. The symmetry-mode approach lets us describe the child structure using this small number of energetically-relevant parameters.

The advantages of the symmetry-mode approach can be summarised in the following five points. Each is exemplified in either Section 3 or Section 4 of the notes.

1. The symmetry-mode approach lets us explore the different possible phase transitions of a material in a concise and systematic way.

2. We can often describe child structures with far fewer parameters than using traditional *xyz* fractional coordinates. This can improve the quality of information extracted from powder data.

3. The magnitude of the parameters we use are naturally defined in a range of ~0–2, where a large magnitude indicates a large structural change. This can help identify which parameters are really relevant in understanding a transition.

4. We can use well-developed web tools to do much of the hard work in understanding symmetry changes at transitions, helping to eliminate errors.

5. Similar ideas can be used to describe structural transitions, order-disorder transitions, magnetic phase transitions, and transitions involving the displacements of (semi) rigid molecules.
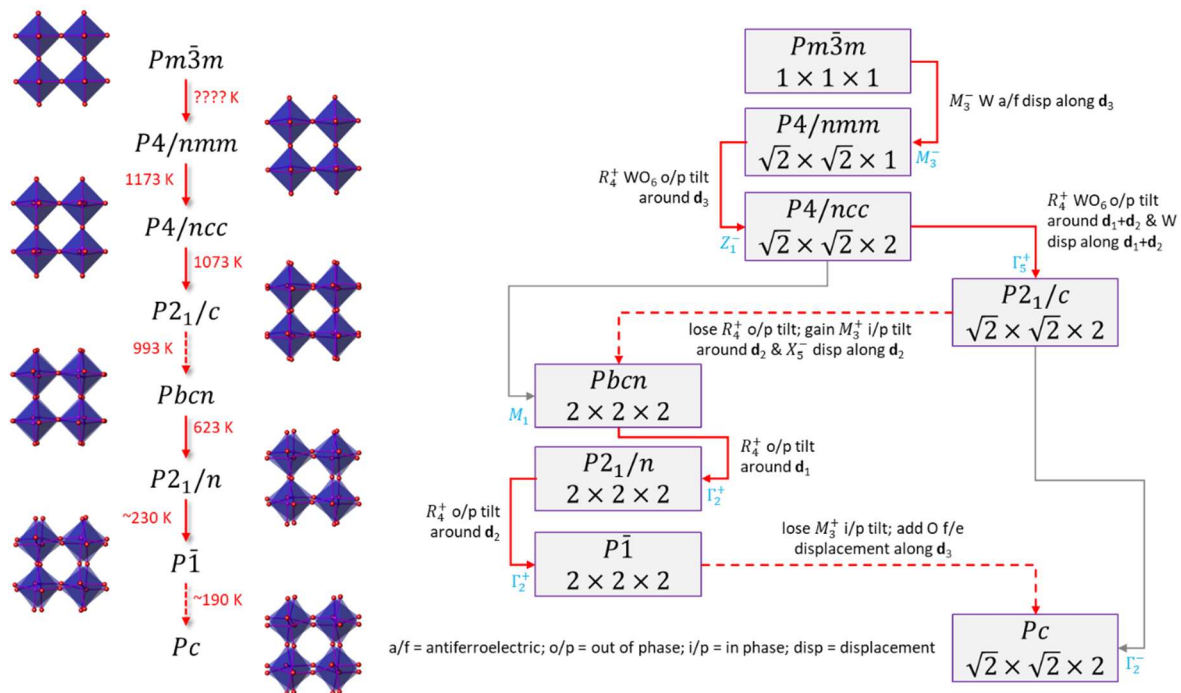
Figure 1: Phase transitions and their symmetry relationships in WO_3. Structures and approximate phase transition temperatures shown on the left, with $WO_{6/2}$ octahedra shown in blue and oxygen atoms in red. Partial group-subgroup tree shown on the right with space-group type and approximate cell parameters relative to the cubic aristotype shown. Only the 7 observed structures of 1427 on the full group-subgroup tree are shown. Red arrows show the actual transition sequence. Solid lines are allowed to be continuous transitions; dashed are discontinuous. Grey line transitions are not observed experimentally. Irrep labels and descriptions are relative to the $Pm\bar{3}m$ parent. d_1–d_3 are basis vectors of the parent cell. Pale blue labels are primary irreps between a specific pair of subgroups.

3. Describing and systematising phase transitions

3.1 WO₃ phase transitions – the problem

The use of symmetry modes to describe phase transitions can be exemplified using WO_3. The structures of the most common polymorphs of WO_3 can be described as a network of corner-sharing $WO_{6/2}$ octahedra. The highest symmetry parent aristotype would be cubic with space group type $Pm\bar{3}m$ and contain perfectly regular WO_6 octahedra with linear W–O–W linkages. This form of WO_3 has never been observed, but we can think of it as the starting point for a series of phase transitions that occur on cooling. These involve W atoms moving off-centre in the octahedra (second order Jahn–Teller distortions) and coupled rotations of the linked octahedra around different axes of the parent structure. Looking down a column of octahedra, these rotations can occur in the same direction for adjacent octahedra (in phase tilts) or in different directions (out of phase tilts), and will be familiar to anybody who has worked on perovskite chemistry.[8-10] The distortions sequentially lower the symmetry, changing both the unit cell and space group as summarized in Figure 1. Understanding the relationships between the various unit cells, symmetry elements, origin choices and fractional atomic coordinates of each of these structures (and which *xyz* coordinates are free to refine in a Rietveld analysis) is hard. It becomes even harder for more complicated structures! Note also from Figure 1 that a space-group type isn't sufficient to specify the structure. For example, space group number 14 appears twice as $P2_1/c$ and $P2_1/n$. To fully describe the symmetry, the space-group type, the unit cell (basis) and the origin of each structure need to be specified.

3.2 Symmetry modes - some background terminology

Although there's a terminology learning curve to overcome, exploring the relationships between WO_3 structures becomes easier using symmetry modes. With online software tools the relationships can be easily explored without a full understanding of the group theory, but we summarise some of the common terminology here for completeness.[11] You should be able to follow most of the rest of the notes independently of this section.

The symmetry operations of a space group are conventionally described by a set of square matrix operations called a *representation*. When these are expressed in their mathematically simplest block diagonal form this is called an *irreducible representation* or *irrep*. A representation has an *order* defined as the number of matrices, and a *dimension* defined by the dimension of the matrices.

A phase transition can always be associated with a *k* point or wave vector in reciprocal space. This *k* point describes where extra reflections will be seen following the phase transition. For example, a phase transition associated with *k* point (½, 0, 0) (the *X* point of $Pm\bar{3}m$) will give a child with extra $(h/2, k, l)$ reflections (or *h'kl* reflections using a doubled *a* axis with $h' = 2h$). For a given parent space group, specifying a *k* point defines a set of irreps. Each of these maps the symmetry elements onto a set of irreducible matrices. When a material undergoes a phase transition some of its symmetry elements are lost and some retained. Those that are retained define what is called the *isotropy subgroup* or *distortion symmetry* of the child.[12] Since each irrep describes a set of parent symmetries that can be broken, they give us a "recipe" for lowering symmetry. The language used is that we superpose one (or more) irreps on the parent space group and this takes us to a specific isotropy subgroup. Within a given isotropy subgroup, many different distortions are possible due to the different structural degrees of freedom the atoms are allowed.

One convenient way to think about a specific distortion is in terms of its *distortion vector*. For the simple case of a single atom moving away from a high-symmetry site in 3D this is very intuitive. If we're thinking of a more complex case involving multiple atoms moving we can use the same idea, but the distortion vector is harder to visualise as it lies in a higher dimensional *vector space* (more formally the carrier space in which the matrices of the space

group representation operate). The distortion vector is invariant under the symmetry operations of the isotropy subgroup. As with any vector, if we can define a *basis* for it, we can describe it in terms of vector components along each of the basis vector directions. In the symmetry-mode approach the irreps are used as a complete and orthogonal basis to describe the distortion vector. The irreps themselves are are simply linear combinations of traditional crystallographic parameters.
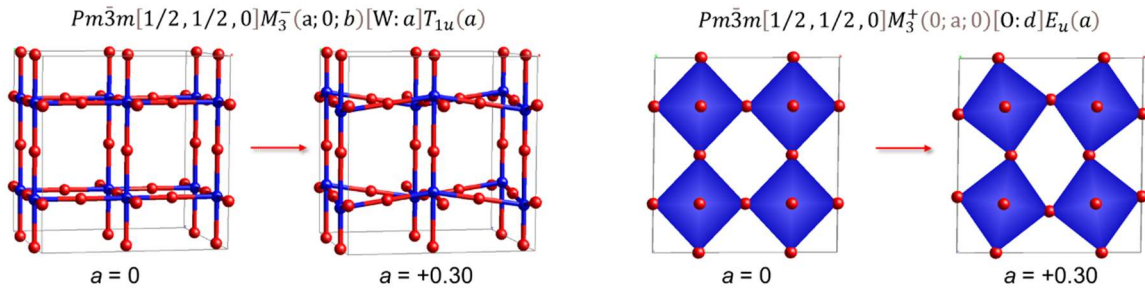
Another important feature of the distortion vector is the *order parameter direction* or *OPD*. An OPD is a specific direction (or subspace) of the generalised distortion space within which each distortion vector represents structures with the same symmetry (remember that each different vector within this subspace represents a different specific distortion). The most general OPD of a three dimensional irrep is expressed as (a, b, c). A vector in this direction will give rise to a distortion symmetry known as the *kernel*. The kernel is the lowest distortion symmetry associated with an irrep. The same three dimensional irrep may have a one dimensional OPD where, for example, b and c are zero or where $a = b$ expressed as $(a, 0, 0)$ or $(a, a, 0)$, respectively. These will lead to an intermediate distortion symmetry that is a subgroup of the parent and a supergroup of the kernel. A simple analogy is to think of moving a single atom in a cubic structure away from $(0, 0, 0)$. If we move it in a general direction to (x, y, z) we will destroy certain symmetry elements; if we move it to (x, x, x) we would retain more symmetry. The variable parameters of an OPD are called *branches*.

In the kernel we can define a *distortion mode* as a vector component along one of the irrep basis vectors; in one of the higher symmetries it may be a linear combination of different irrep basis vectors. The ISODISTORT definition of an *order parameter* is a distortion vector along a specific OPD of a specific irrep at a specific k-point of the parent symmetry. The parameters used to specify it are the individual distortion mode amplitudes (one for each branch of the OPD) and these are therefore *order parameter component*s. This is the link to the more familiar concept of the order parameter of a phase transition as a quantity that is zero above the transition and evolves in either a *continuous* or *discontinuous* way to a non-zero value below the transition.[10] The magnitude of the distortion vector, which is itself defined by mode amplitudes, is the order parameter that describes the free energy associated with the transition.

Putting all this together, during a symmetry-mode refinement we will refine the amplitude of each symmetry mode (a single parameter) which may influence the fractional coordinates of multiple atoms. ISODISTORT identifies these modes by a label of the form $Pm\bar{3}m[1/2,1/2,1/2]R_4^+(a,0,b)[O1:d:dsp]E_u(a)$. Here $Pm\bar{3}m$ is the parent space group, $[1/2,1/2,1/2]$ the k point (which is the R point of $Pm\bar{3}m$), R_4^+ is the three dimensional irrep label using Miller and Love notation[13] and $(a,0,b)$ is the two dimensional order parameter direction. The final part of the label gives the Wyckoff site of the parent atom (O1) and the spectroscopic label for the Wyckoff site point group irrep that induces the distortion. dsp labels a displacive mode, while *occ*, *mag*, or *rot* would label occupancy, magnetic or rotational modes. In some cases an additional order parameter number is appended (_1, _2) to distinguish different modes with the same local point group irrep. The final labels 'a' and 'b' distinguish the two branches of the two dimensional order parameter. Sometimes you will see semicolons in OPD label, not commas. These are used for cases where irreps of different symmetry equivalent k points in the parent group (e.g. $k = (1/2,1/2,0); (1/2,0,1/2); (0,1/2,1/2)$ for the M point of $Pm\bar{3}m$) are active. In ISODISTORT amplitudes of displacive modes are defined as the square root of the sum of the squares of the mode-induced displacements within the primitive child cell in Å, and typically vary between around -2 and $+2$; the larger the amplitude the larger the structural distortions.

3.3 WO₃ phase transitions – the isotropy group subgroup tree

From the previous sections we have the language in place to describe the WO_3 phase transitions using symmetry-modes. We can start by taking the parent $Pm\bar{3}m$ structure and superposing an M_3^- irrep to lower the symmetry. The OPD has six choices, each of which would lead to a subgroup with a different space-group type, origin choice and basis combination. The OPD that occurs is labelled $P1(a; 0; 0)$ and moves alternating W atoms up or down the c-axis of the parent unit cell leading to an antiferroelectric structure with a $\sim\sqrt{2}a \times \sim\sqrt{2}a \times \sim a$ (hereafter simplified to $\sqrt{2} \times \sqrt{2} \times 1$) unit cell and space-group type $P4/nmm$ (the structure is drawn in Figure 2). We discuss below how this could be determined experimentally, but note that three structural parameters (a single mode amplitude for W and O and a c/a cell strain ratio) fully-describe the structure. The next two transitions involve out-of-phase rotations of WO_6 octahedra around different axes. Both can be described with R_4^+ distortions relative to the parent structure (though note that irrep labels change when the unit cell changes). OPD $R_4^+(b, 0, 0)$ leads to the $P4/ncc$ structure and the more general OPD $R_4^+(b, c, c)$ to the lower-symmetry $P2_1/c$ structure. The specific combinations of M_3^- and R_4^+ are sufficient to define the symmetry of each structure, and these can be described as *primary irreps*. When they are active, other irreps are activated (e.g. X_4^-, X_5^-, M_5^-, R_3^+, R_5^+ in the $P2_1/c$ structure) which are called *secondary irreps*. The corresponding modes may or may not have significant amplitude.

$Pm\bar{3}m[1/2, 1/2, 0]M_3^-(a; 0; b)[W: a]T_{1u}(a)$ $Pm\bar{3}m[1/2, 1/2, 0]M_3^+(0; a; 0)[O: d]E_u(a)$

$a = 0$ $a = +0.30$ $a = 0$ $a = +0.30$

Figure 2: an M_3^- mode describing antiferroelectric displacement of W atoms and an M_3^+ mode describing in-phase tilting of octahedra. A single mode amplitude displaces multiple atoms.

The irreps leading to the other polymorphs are summarised in Figure 1. Note that in some cases WO_3 undergoes transitions between structures which don't have a direct group-subgroup relationship. One example is the $\sim$1000 K $P2_1/c$ structure on the right-hand part of the tree, which on further cooling has to "move up" the group-subgroup tree by losing some distortions (one of the R_4^+ tilts) before other distortions are introduced and it descends again down the left-hand pathway. Similarly, once WO_3 reaches the $P\bar{1}$ structure on the left-hand pathway it jumps back to the right-hand pathway on further cooling. We can think of this as the structure exploring an energy-lowering route on cooling which turns out to be a cul-de-sac, and it has to backtrack to reach its global energy minimum on further cooling. From the symmetry properties of the irreps we can predict whether a transition can be continuous (solid arrows) or has to be discontinuous (dashed arrows). In a powder experiment a discontinuous transition would lead to abrupt changes in cell parameters. This occurs, for example, for the $P\bar{1}$ to Pc transition on cooling that was discussed in the notes on parametric refinement.

The irrep labels can also contain useful information about property changes. For example, the hypothetical transition from $P2_1/c$ to Pc involves the Γ_2^- irrep. Here the "−" flags a loss of an inversion centre, and WO_3 goes from a centrosymmetric-non-polar to polar (pyroelectric or potentially ferroelectric) form. A Γ_1^+ mode in any child represents a structural distortion that was also allowed in the parent.

4. Example applications of symmetry-mode refinements

Each of the structural transitions of Figure 1 increases the structural complexity of WO_3. In the room temperature $P2_1/n$ structure there are 24 structural degrees of freedom (plus cell parameters). These could be described with 24 *xyz* fractional atomic coordinates or 24 mode amplitudes. As shown in the next section, it turns out that with the symmetry-mode approach only a few of these (5 to 7) are actually important, leading to an efficient structure description.

Similarly, if the symmetry was lowered further to a $2 \times 2 \times 2$ cell with space group $P1$, there would be 96 possible modes. If we had a powder pattern of WO_3 and could decide which of these 96 modes are actually needed to fit the data, we could determine the space group symmetry (from which modes/irreps are active) and the structure (from the amplitudes of these active modes) simultaneously.

The complexity of analysing structures with these types of transitions can be appreciated by working out all the possible subgroups between the $Pm\bar{3}m$ parent and this hypothetical $P1$ structure, which we'll call the *base child*. It turns out that there are 1427 possibilities! Another way of analysing a powder pattern of WO_3 to determine the true structure would be to test each of these 1427 models in turn and decide which is best.

The three key ideas of the previous paragraphs are exemplified in the following sections.

4.1 Symmetry-mode refinements – reducing parameters

Figure 3 shows the results of a Rietveld fit to 1123 K X-ray data of WO_3 in its $P4/ncc$ $\sqrt{2} \times \sqrt{2} \times 2$ form. In this case analysis using ISODISTORT (explicit details on how this is done are at https://topas.webspace.durham.ac.uk/tutorial_isoriet_wo3_advanced/) produces a Rietveld instruction file showing there are three allowed mode amplitudes. As discussed above, two of these describe octahedral distortions and the third octahedral tilting. The bottom Rietveld fit in Figure 3 uses a simple cubic model. The middle fit allows the *a* and *c* cell parameters to differ, and explains most of the strong peaks. This constrained fit (mode amplitudes all zero) is actually equivalent to a $P4/nmm$ model with a $1 \times 1 \times 1$ unit cell. Note that a symmetry-mode refinement with the amplitudes of modes of specific irreps fixed at zero mimics a higher-symmetry space group. The third fit allows the three mode amplitudes to refine and gives an excellent agreement between observed and calculated data.
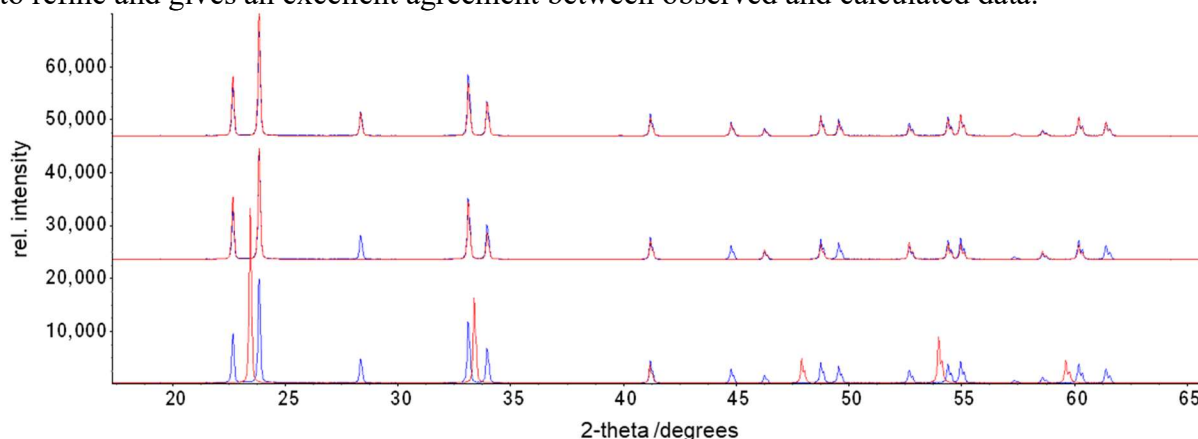
Figure 3: Rietveld fit to 1123 K data of WO_3. Lowest fit uses a cubic model. Middle fit use a tetragonal model with mode amplitudes at zero, several super structure reflections are not explained. Top fit refines the three symmetry-mode amplitudes.

In this case three parameters are needed in either a symmetry-mode or conventional *xyz* description. However, Figure 4 shows a fit to data of the room temperature $P2_1/n$ monoclinic structure. Here the lower plot shows a conventional Rietveld using 24 *xyz* parameters (R_{wp} = 9.0%) and the upper fit uses just five distortion mode amplitudes and gives an essentially

equivalent fit with $R_{wp} = 9.2\%$. These amplitudes describe the various octahedral distortions and tilts that occur. Even in a combined X-ray and neutron fit, the data can be well-described with just seven mode amplitudes, showing how concise the symmetry-mode description can be. Step-by-step instructions on how to perform the fit of Figure 4 are available online (https://topas.webspace.durham.ac.uk/tutorial_isoriet_wo3_simple/).
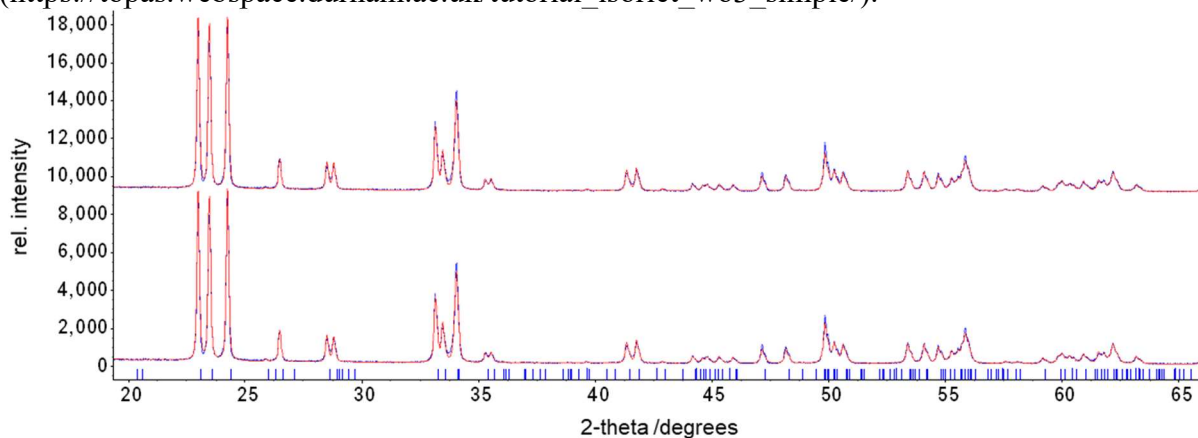
Figure 4: Rietveld fit to 300 K X—ray data of WO_3. Upper fit uses 5 symmetry-mode amplitudes. Lower fit uses 24 *xyz* fractional atomic coordinates.

4.2 Parameter conciseness and determining symmetry

Another way to demonstrate the conciseness of the symmetry-mode description is shown in Figure 5.[14] In this analysis we ignored the fact that the true space group of WO_3 is $P2_1/n$ and assumed a $2 \times 2 \times 2$ cell with $P1$ symmetry, which has 96 possible mode amplitudes (or 96 *xyz* coordinates). We then did a "mode inclusion" test in which we refined each one of the 96 mode amplitudes in turn against X-ray and neutron data and selected the mode that gave the lowest R_{wp}. We then refined this mode with each of the other 95 modes in turn to obtain the best two-mode description. This was repeated until all 96 modes were included (4657 separate refinements in total). We also did the same thing but using individual *x*, *y* or *z* fractional coordinates instead of mode amplitudes. To check reversibility, we repeated each process in reverse by starting with all 96 parameters included, then sequentially removing the single parameter with the least impact on the fit.
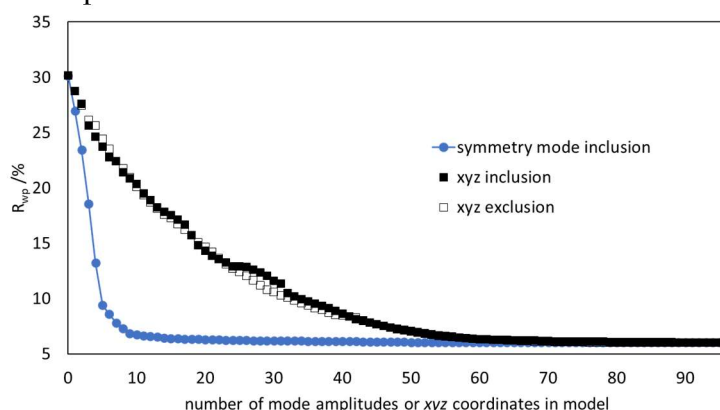
Figure 5: R_{wp} values obtained as a function of the number of structural degrees of freedom using either symmetry modes or *xyz* parameters. Values from simultaneous fit to X-ray and neutron data.

Figure 5 plots the R_{wp} values from this analysis and shows how efficient the mode parameter set is compared to *xyz* in this test. We see that after adding ~7 modes there is no further

improvement in fit with the symmetry-mode description, whereas over 60 *xyz* parameters are required for a similar fit.

By looking at which seven modes are important we can do more. It turns of that they belong to a small number of irreps ($R_4^+, M_3^+, M_3^-, X_5^+, X_5^-$). If we take the irreps and OPDs and superpose them on the parent structure it uniquely defines the correct $P2_1/n$ space-group type, basis and origin. The space group and structure of the sample have therefore been "refined" simultaneously from the data.

There are more general ways we can do the same thing using genetic algorithms in which we describe the active modes in the structure using a series of 96 1's and 0's [00101100…..] for active/inactive. By testing populations of different structures against the data, ranking them by R_{wp} then mutating and breeding them using Darwinian evolution ideas, we can again identify the important modes and determine the symmetry and structure simultaneously.[14]

4.3 Exhaustive searching of group-subgroup trees – Bi₂Sn₂O₇

$Bi_2Sn_2O_7$ is a published example where the exhaustive searching of group-subgroup trees was necessary to understand its structures, and where complicated crystallography ultimately lead to a simple final picture.[15] At high temperature $Bi_2Sn_2O_7$ is a cubic pyrochlore (space group $Fd\bar{3}m$, $a \approx 10.75$ Å) with just one refinable atomic coordinate. On cooling it undergoes phase transitions to a β- then α-polymorph and becomes significantly more complex. The literature contains many wrong descriptions of both structures.

The true structures were determined with a symmetry-mode approach. First, it was found that all the features of the X-ray and neutron high resolution powder patterns (splittings, superstructure reflections) of all phases could be described with a $P1$ model with a $2 \times 2 \times 2$ superstructure. This was defined as the base child, and a group-subgroup tree produced using ISODISTORT contained 547 possible candidate structures between the parent and base child. All structures were refined against neutron and X-ray data, and the candidate with a low R_{wp} and a sensible number of parameters determined for both α and β. All 547 fits of α- $Bi_2Sn_2O_7$ are summarized in Figure 6a–c.
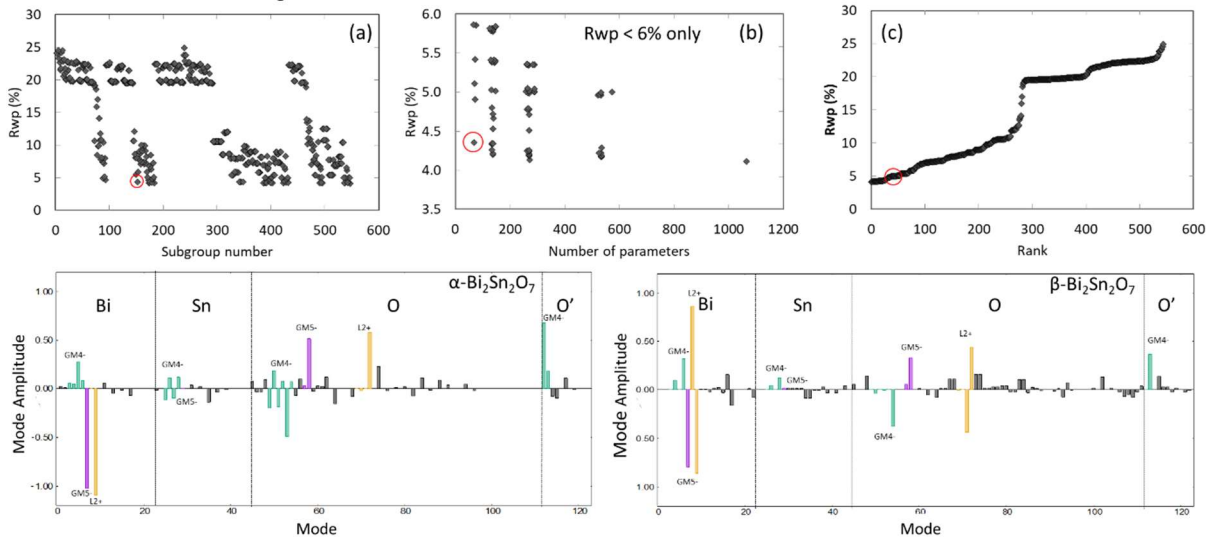
Figure 6: Exploration of group-subgroup trees for α-Bi₂Sn₂O₇ by Rietveld refinement. Panels (a), (b) and (c) plot R_{wp} for the 547 possible models by subgroup number, number of independent parameters and rank order, respectively. The best model has a low R_{wp} for a small number of parameters and fits all aspects of the experimental data. The lower panels show how the structures of α- and β-Bi₂Sn₂O₇ can be compared by plotting the amplitudes of the distortion modes relative to the parent cubic structure in a common subgroup. The key difference is in the active L_2^+ OPD. α has $L_2^+(0, a, 0, 0)$ and β $L_2^+(-a, a, 0, 0)$; these describe distinct shift patterns of Bi^{3+} cations.

The β structure turns out to have space-group type *Aba*2 with $a = 7.57$ Å, $b = 21.41$ Å, $c = 15.12$ Å and the α structure has space-group type *Pc* with $a = 13.15$ Å, $b = 7.54$ Å, $c = 15.08$ Å, $β = 125.01°$. By examining the active modes in each (particularly a $L_2^+(0, a, 0, 0)$ in α and $L_2^+(-a, a, 0, 0)$ in β) a simple picture of the phase transitions in terms of specific shifts of the active lone pair Bi^{3+} cation emerged. This complex behaviour was later supported by DFT studies.[16]

The work was all done using TOPAS[17-18] in a fully automated way using Python scripts. Nowadays it can be done using a single TOPAS input file and the internal #list syntax to perform all the refinements.

5. Other distortion modes

The examples discussed in these notes involve atomic displacements which have the tensor properties of polar vectors. A similar language can be used to describe phase transitions involving site occupancies, which are scalar parameters. Magnetic phase transitions, which involve the ordering of magnetic moments with both direction and spin, can be described using axial vectors or pseudo vectors.[19-20] We can think of axial vectors as rotating cylinders describing the moment orientation through the vector orientation and its "up/down" nature through the direction of rotation (clockwise or anti-clockwise). Magnetic structures can therefore be described in terms of the amplitude of magnetic symmetry modes. Our view of axial vectors also suggests how an analogous language can be used to describe transitions involving molecular rotations. The direction of the axial vector can be used to specify the axis of molecular rotation, and its length the magnitude of the angle of rotation. Symmetry aspects of the phase transitions of molecular materials can then be explored in similar ways to those described above, with low symmetry structures described in terms of the parent plus the amplitude of Rietveld-refined molecular distortion modes.[5, 21-22]

6. Conclusions and what next

Try the tutorials at https://topas.webspace.durham.ac.uk/topas_user_menu/. Several of these are based on the WO_3 example in these notes. There are step-by-step notes on using ISO-DISTORT to understand transitions and on performing Rietveld symmetry-mode refinements.

7. Acknowledgements

8. References

1. Campbell, B. J.; Evans, J. S. O.; Perselli, F.; Stokes, H. T., Rietveld refinement of structural distortion-mode amplitudes. *IUCr Crystallographic Computing Newsletter* **2007,** *8*, 81-95.
2. Perez-Mato, J.; Orobengoa, D.; Aroyo, M., Mode crystallography of distorted structures. *Acta Crystallographica Section A: Foundations of Crystallography* **2010,** *66* (5), 558-590.
3. Campbell, B. J.; Stokes, H. T.; Tanner, D. E.; Hatch, D. M., ISODISPLACE: a web-based tool for exploring structural distortions. *Journal of Applied Crystallography* **2006,** *39* (4), 607-614.

4.   Dinnebier, R. E.; Leineweber, A.; Evans, J. S. O., *Rietveld Refinement, Practical Powder Diffraction Pattern Analysis using TOPAS*. De Gruyter: 2018; p 331.

5.   Müller, M.; Dinnebier, R. E.; Dippel, A.-C.; Stokes, H. T.; Campbell, B. J., A symmetry-mode description of rigid-body rotations in crystalline solids: a case study of $Mg(H_2O)_6RbBr_3$. *Journal of Applied Crystallography* **2014,** *47* (2), 532-538.

6.   Kerman, S.; Campbell, B. J.; Satyavarapu, K. K.; Stokes, H. T.; Perselli, F.; Evans, J. S. O., The superstructure determination of displacive distortions via symmetry-mode analysis. *Acta Crystallographica Section A* **2012,** *68* (2), 222-234.

7.   Landau, L. D.; Lifshitz, E. M., *Course of theoretical physics*. Elsevier: 2013.

8.   Glazer, A. M., The classification of tilted octahedra in perovskites. *Acta Crystallographica Section B: Structural Crystallography and Crystal Chemistry* **1972,** *28* (11), 3384-3392.

9.   Howard, C. J.; Stokes, H. T., Group-theoretical analysis of octahedral tilting in perovskites. *Acta Crystallographica Section B: Structural Science* **1998,** *54* (6), 782-789.

10. Woodward, P. M.; Karen, P.; Evans, J. S. O.; Vogt, T., *Solid State Materials Chemistry*. Cambridge University Press: Cambridge, 2021; p 687.

11. Bradley, C.; Cracknell, A., *The mathematical theory of symmetry in solids: representation theory for point groups and space groups*. Oxford University Press: 2010.

12. Hatch, D. M.; Stokes, H. T., *Isotropy subgroups of the 230 crystallographic space groups*. World Scientific: 1989.

13. Miller, S. C.; Love, W. F., Tables of irreducible representations of space groups and co-representations of magnetic space groups. **1967**.

14. Lewis, J. W. Symmetry methods for understanding structures of inorganic functional materials. Durham University, 2018.

15. Lewis, J. W.; Payne, J. L.; Evans, I. R.; Stokes, H. T.; Campbell, B. J.; Evans, J. S. O., An Exhaustive Symmetry Approach to Structure Determination: Phase Transitions in $Bi_2Sn_2O_7$. *Journal of the American Chemical Society* **2016,** *138* (25), 8031-8042.

16. Rahim, W.; Skelton, J. M.; Savory, C. N.; Evans, I. R.; Evans, J. S.; Walsh, A.; Scanlon, D. O., Polymorph exploration of bismuth stannate using first-principles phonon mode mapping. *Chemical science* **2020,** *11* (30), 7904-7909.

17. Coelho, A. A., TOPAS and TOPAS-Academic: an optimization program integrating computer algebra and crystallographic objects written in C++. *Journal of Applied Crystallography* **2018,** *51* (1), 210-218.

18. Coelho, A. A.; Evans, J. S. O.; Evans, I. R.; Kern, A.; Parsons, S., The TOPAS Symbolic Computation System. *Powder Diffraction* **2011,** *26* (4), S22.

19. Perez-Mato, J.; Ribeiro, J.; Petricek, V.; Aroyo, M., Magnetic superspace groups and symmetry constraints in incommensurate magnetic phases. *Journal of Physics: Condensed Matter* **2012,** *24* (16), 163201.

20. Wills, A., Magnetic structures and their determination using group theory. *Le Journal de Physique IV* **2001,** *11* (PR9), Pr9-133-Pr9-158.

21. Liu, H.; Zhang, W.; Halasyamani, P. S.; Stokes, H. T.; Campbell, B. J.; Evans, J. S. O.; Evans, I. R., Understanding the Behavior of the Above-Room-Temperature Molecular Ferroelectric 5, 6-Dichloro-2-methylbenzimidazole Using Symmetry Adapted Distortion Mode Analysis. *J. Am. Chem. Soc.* **2018,** *140* (41), 13441-13448.

22. Liu, H.-Y.; Gutmann, M. J.; Stokes, H. T.; Campbell, B. J.; Evans, I. R.; Evans, J. S. O., Supercolossal Uniaxial Negative Thermal Expansion in Chloranilic Acid Pyrazine, CA-Pyz. *Chemistry of Materials* **2019,** *31*, 4514-4523.